

Investigation of Constant Stack Pressure on Lithium-Ion Battery Performance

Aiden Leonard^a, Brady Planden^a, Katie Lukow^{a*}, Denise Morrey^a

^aHigh Voltage Energy Storage Group, School of Engineering, Computing, and Mathematics, Oxford Brookes University, Oxford, UK, OX33 1HX

*Correspondence: clukow@brookes.ac.uk

Abstract

Current research involving applying stack pressure to lithium-pouch cells has shown both performance and lifetime benefits. Fixtures are used to mimic this at the cell level and conventionally prescribe a constant displacement onto the cell. This increases stack pressure, but also causes pressure to vary. Despite this, applying an initial stack pressure improves cell conductivity and cell lifetime [1, 2]. In this work, a fixture was designed that applies constant pressure to the cell independent of displacement. The fixture uses pneumatics to apply a constant stack pressure independent of elastic and plastic swelling. Cells constrained by the constant pressure fixture and a conventional displacement based fixture were evaluated using a Hybrid Pulse Power Characterisation (HPPC) test to measure internal resistance and maximum deliverable power. Multiple stack pressures were applied to investigate the variance in pressure over operational conditions and performance between constant pressure and constant displacement based methods. All tests were further compared to a control case with no applied stack pressure. The constant pressure based method reduced pressure variation during charging and discharging, reduced the discharge impedance and improved discharged power, but did not improve charge performance. Discharge performance benefits from constant pressure could influence pack design to improve vehicle performance.

Keywords: Lithium-ion battery, Pack design, Stack pressure, Battery performance

Abbreviations

Symbol	Definition
Q_{Δ}	Capacity loss/gain (Ah)
CPF	Constant pressure fixture
DCIR	Direct current internal resistance
D_{\max}	100% Maximum discharge current
$D_{\max/2}$	50% Maximum discharge current
HPPC	Hybrid pulse power characterisation
MBPF	Modular battery pressure fixture

1 Introduction

Lithium-ion cells have quickly become to standard for many industries requiring reliable and efficient battery storage. Pouch cells provide a unique solution for increased packaging density and increased power density when compared to most conventional cylindrical cells; however, they bring additional challenges as well. Most notably, is the requirement of external stack pressure to prolong life and optimise performance. Stack pressure has been applied to pouch cells via various methods, generally falling into two categories, fixed displacement and constant pressure. Conventionally, fixed displacement is achieved by constraining the orthonormal expansion of the cell through rigid plates. Constant pressure based methods conventionally allow for expansions of the cell through the additions of varying-stiffness foam or spring elements [1, 2]. Pressure has been shown to improve the interfacial surface area between the negative electrode, positive electrode, and separator, thus decreasing the ionic resistivity [3–6]; however, reaches a critical value where additional mechanical stress has been shown to reduce active electrode material, reducing the performance of cells [5–8]. Stack pressure varies elastically throughout the battery’s state-of-charge for a corresponding fixed displacement fixture due to lithiation of the anode and increases over time due to anode growth [1, 9–12]. Development of a stack pressure method that is cell thickness agnostic is the aim of this work, potentially providing performance benefits through increasing the positive effects of pressure without causing damage through uncontrolled pressure increases due to ageing [1].

Current research involving applying stack pressure to pouch cells has resulted in immediate and long-term performance benefits. A study conducted by Müller et al. [5] utilised parallel plates with springs to apply pressure ranging from 0-0.84 MPa to both a full NMC/graphite cell and the individual cathode, anode, and separator. The results show an optimal pressure to minimise separator resistivity from 0.1-0.6 MPa, and an increasing relationship between the electrode resistances and pressure. At the cell level, stack pressure increased the charge transfer resistance but decreased the high frequency resistance. Pressures above 100 kPa have been seen to improve conductivity for future cell materials, such as lithium-metal and solid electrolytes [13–15]. Doux et al. [13] explored the effect of stack pressure on a sulfide electrolyte solid-state battery and tested pressures from 5 MPa to 70 MPa. Electrode conductivity improved for pressures up to 70 MPa, while discharge capacity decreased at the upper limit of pressure tested. A study conducted by Louli et al. [16] found that 1.7 MPa of stack pressure provided the highest performance for a lithium-metal negative electrode cell using a liquid electrolyte; However, the study reported a 50-300% change in pressure from the thickness change of the cell during charging and discharging. A hybrid lithium-ion/lithium-metal cell was also found to benefit from 1.2 MPa of applied stack pressure, [17] enabling a dendrite suppression mechanism which corresponds to cycle-life benefits. For lithium-ion cells, the SEI layer has been shown to grow over the life of the cell, increasing impedance and decreasing usable capacity [18]. Stack pressure is shown to reduce capacity fade through suppressing delamination of electrodes, gassing of the electrolyte, and SEI layer growth

68 [7, 11]. Hahn et al. [1] presents a varying applied stack pressure between 38-580 kPa,
69 improved capacity retention from 95% to 99% after 70 days of calendar ageing. Further
70 studies support the discharge capacity improvement gained from reducing the applied
71 current density due to pressure application [19, 20]. Along with capacity improvements,
72 increasing stack pressure for lithium-ion cells has shown to improve interfacial contact
73 of electrodes to the separator [7]. Since non-flat electrode surfaces have a limited con-
74 tact surface area, creating a more ideal flat surface contact between elements in cells
75 results in immediate performance benefits. With elastic contact on rough surfaces, the
76 contact area increases proportionally to the load [21–23]. Improving interfacial surface
77 area contact immediately reduces the current density in the localised region [20]. The
78 larger interaction area between electrodes also reduces the effective ion path length, fur-
79 ther reducing impedance [15]. These performance benefits from applying a stack pressure
80 influence current and next-generation battery pack design. Current modules have two
81 main methods of applying stack pressure. Modules fix the outer dimensions of cells using
82 cylindrical cells or volumetrically constricted groups of pouch cells [24]. Furthermore,
83 deformable materials are used between cells to reduce pressure variance from expansion
84 and contraction [1]. Based on current research on lithium-metal [14, 17] and Silicon [13,
85 19, 25] cells, future battery packs will likely benefit from higher stack pressure applied
86 to cells. Studies look for performance benefits by either constraining thickness or using
87 spring-like elements.

88 Basic fixtures use flat parallel plates and apply pressure by using bolt torques to
89 clamp the cell between the plates [13, 26, 27]. However, because the width between
90 each plate is essentially fixed, stack pressure varies during charging and discharging due
91 to elastic swelling, with SOC due to differences in electrode volumes, and over time
92 increases due to negative electrode growth [1, 28–30]. Hahn et al. [1] studied the long-term
93 effects of mechanical pressure by using a hydraulic cylinder and porous foam as a spring
94 element. This approach provided flexibility in altering pressure to model cell elasticity
95 as a spring-like element; however, this study did not observe the effects of constant
96 pressure due to the pressure increase over cell lifetime corresponding with cell thickness
97 growth. Other novel fixtures [2, 17], utilise buffer layers of foam to dampen the thickness
98 growth; however, stack pressure then becomes dependent on the compressive stiffness of
99 the foam. Conventionally, to apply a constant, high amplitude pressure, three methods
100 are utilised: electric, hydraulic, or pneumatic actuation. Using pneumatic actuation has
101 conventionally provided advantages of low viscosity and compressibility, thus minimising
102 the pressure variance to a corresponding volume change; however, a system leakage is
103 common causing the need for an air compressor. Hydraulic actuation commonly provides
104 the lowest cost with minimal leakage under normal operation; however, even minimal
105 hydraulic leaks could cause an electrical short circuit for the tested battery. Electric
106 actuation can provide a constant pressure over long periods, but the corresponding high
107 power consumption and pressure dependency on motor and sensor accuracy are not ideal.
108 Due to the above limitations, hydraulic and electric actuation were ruled out due to the
109 risk of short circuits and high costs. As pneumatic actuation does not suffer from these

110 limitations and has a relatively low cost, it was selected for this work.

111 The performance impacts of constant pressure on lithium-ion pouch cell is relatively
112 unknown. As previously discussed, constant pressure research has been previously focused
113 on low amplitude (<40 N Jiang et al. [2]) or amplitudes above 1 MPa for lithium-metal
114 chemistries [14]. In this paper, a constant pressure fixture (CPF) utilising pneumatic ac-
115 tuation for stable pressure values independent of elastic and plastic swelling is presented.

116 **2 Methodology**

117 The following section provides an overview of the fixture design, data acquisition and
118 analysis methods, and experimental methods.

119 **2.1 Fixture Design**

120 A novel fixture was designed to maintain a constant face pressure during cell cycling using
121 a pneumatic actuator. The design targeted up to 180 kPa for testing current-generation
122 liquid electrolyte cells with the ability to replace the pneumatic actuator to allow for
123 larger face pressures if required. Figure 1 presents the design of the proposed constant
124 pressure fixture (CPF) and the reference constant displacement fixture, referred to as the
125 modular battery pressure fixture (MBPF). The fixture applies a constant stack pressure
126 to the face of the battery through the pneumatic actuator and is transferred through two
127 carbon-inlaid 3D-printed plates. This material electrically isolates the battery to prevent
128 the risk of short circuits and provides sufficient stiffness to improve pressure distribution.
129 The ball-and-socket joint provides rotational freedom, allowing the contact between the
130 cell and the pressure plates to be uniform and less dependent cell swelling. Two TE FX29
131 load cells measure force, that are monitored through a Teensy 4.1 board and recorded
132 onto a microSD card.

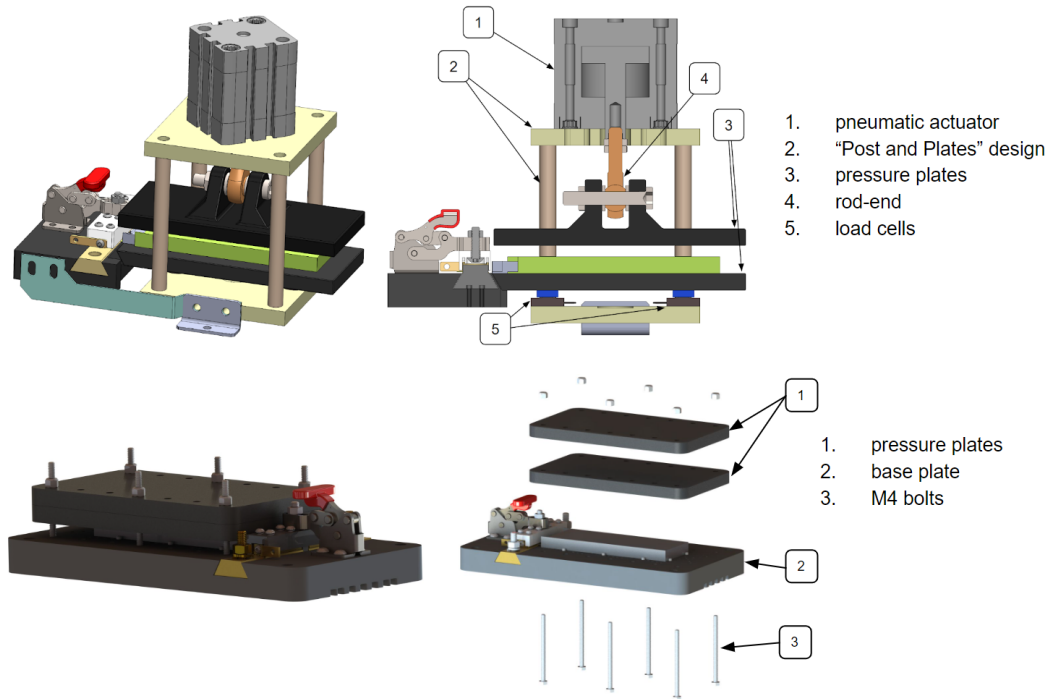


Figure 1: CPF (top) and MBPF [31] (bottom) CAD, with crucial design elements enumerated.

133 Results in this work were compared against two other fixture methods. A baseline
 134 condition of no external stack pressure was first tested. Second, a constant displacement
 135 fixture developed by the High Voltage and Energy Storage group as shown in figure 1
 136 [31]. The fixture applies stack pressure through two plates fastened at up to 6 locations,
 137 measured through TE FX29 sensors similar to the constant pressure fixture. Further
 138 information can be found in the GitHub repository. As discussed, stack pressure was
 139 applied through a pneumatic piston connected to an air reservoir to counteract cell swell
 140 and minor leaks within the system. Initial testing showed that pressure was maintained
 141 over a 48 hour period.

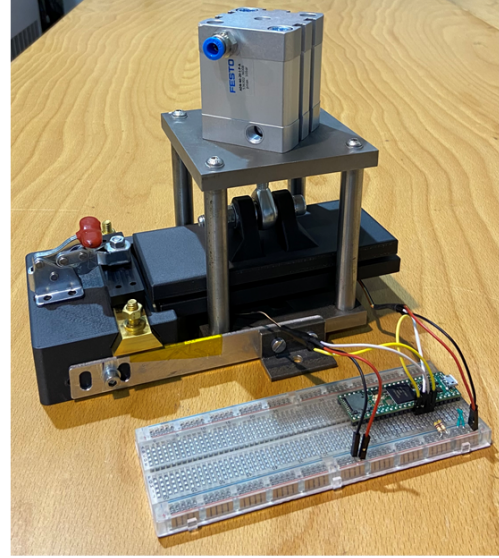
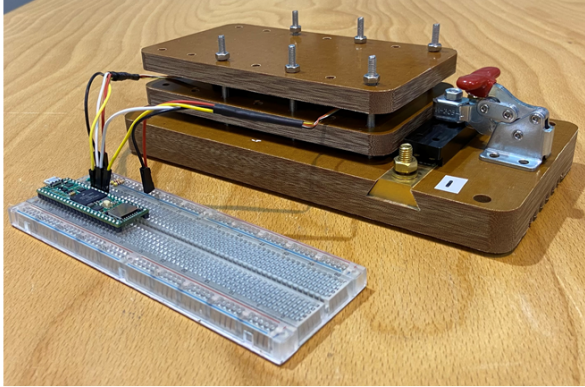


Figure 2: Test measuring pressure variation over 24 hours between the MBPF (left) and CPF (right).

142 Two TE FX29 load cells were placed between the lower cell plate and the base of the
 143 test fixture. The load cells were connected to a Teensy 4.1 microcontroller that recorded
 144 the values throughout the test via a microSD card. A type-T thermocouple was placed
 145 on the body of the cell located near the cell tabs. An Arbin LBT-21084-HC cell cycler
 146 was used to perform the experiments.

147 2.2 Test method

148 A 3.7 Ah LCO/graphite pouch cell was used throughout this study with specifications as
 149 defined in Table 1.

Table 1: Rated Cell Specifications [32]

Cell	Chemistry	Nominal Voltage [V]	Initial AC Impedance $m\Omega$	Initial DC Resistance $m\Omega$	Nominal Capacity [Ah]	Energy Density [Wh/kg]	Power Density [W/kg]
Melasta SLPB 7336128HV	LCO / NMC	3.8	< 2.6	N/A	3.7	204	5043

150 A Hybrid Pulse Power Characterisation (HPPC) test was conducted every 5% state-
 151 of-charge, beginning at 100% SOC. A pulse profile a 10 second load followed by a 40
 152 second rest was completed as shown in Figure 3.

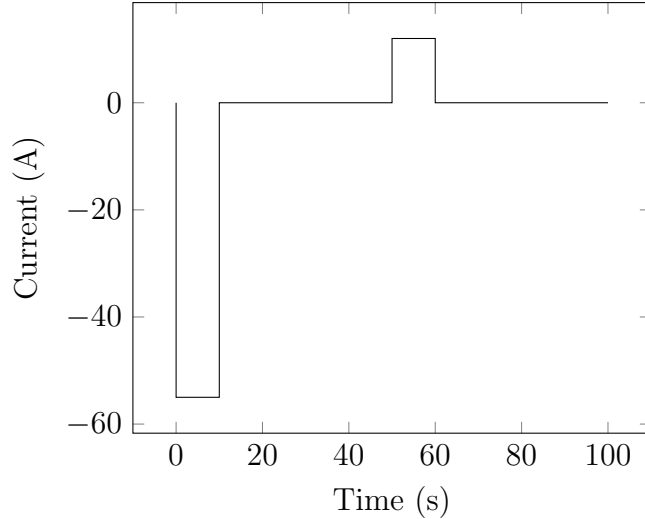


Figure 3: HPPC Pulse Profile

153 The test was performed at the maximum discharge and maximum charge as shown
 154 in the figure above. Tests were also completed at half these values. Stack pressures were
 155 compared at 30, 60, and 90 kPa alongside a benchmark test that had no stack pressure
 156 applied. Ambient temperature was fixed at 25°C for all conditions.

157 3 Results and Discussion

158 3.1 Pressure Variance

159 Pressure data was recorded for all 21 experiments. For all experiments, pressure increased
 160 respective to both SOC and pulse current. Pressure varied more with the MBPF over
 161 the tests, for 60 kPa of initial stack pressure, the MBPF pressure varied from 44-171
 162 kPa, while the CPF cell pressure varied from 54-69 kPa. The measured stack pressure
 163 increased during both the charge and discharge current pulses (Figure 4). The relationship
 164 between pressure and SOC for each pulse (Figure 5) shows The CPF having a linear slope
 165 with an increased slope above 60% SOC; however, the MBPF's fixed displacement method
 166 resulted in a large pressure vs SOC slope compared to the CPF. While the MBPF provides
 167 poor performance across the full SOC operational range, within 30-60% it has a small
 168 range of potential acceptable usage with a delta of 26.7-56.7%. The MBPF pressure vs
 169 SOC slope was lower for 90 kPa of initial stack pressure at above 80% SOC, compared to
 170 30 kPa and 60 kPa. This could be due to physical deformation of the cell orthogonal to
 171 the clamping force, or due to deformation of the MBPF itself. According to Hahn et al.
 172 [1] and Li et al. [6], increased cell deformation occurs above 1000 kPa, therefore the most
 173 likely cause of the decline in slope of pressure vs SOC is the elastic creep of the MBPF
 174 fixture itself. For the MPBF, significant changes in pressure occur at approximately 30%
 175 and 60% SOC. This is expected to correspond with the knee points in the open-circuit
 176 potential as per Figure 4, as the thickness of the cell aligns with the voltage vs SOC curve

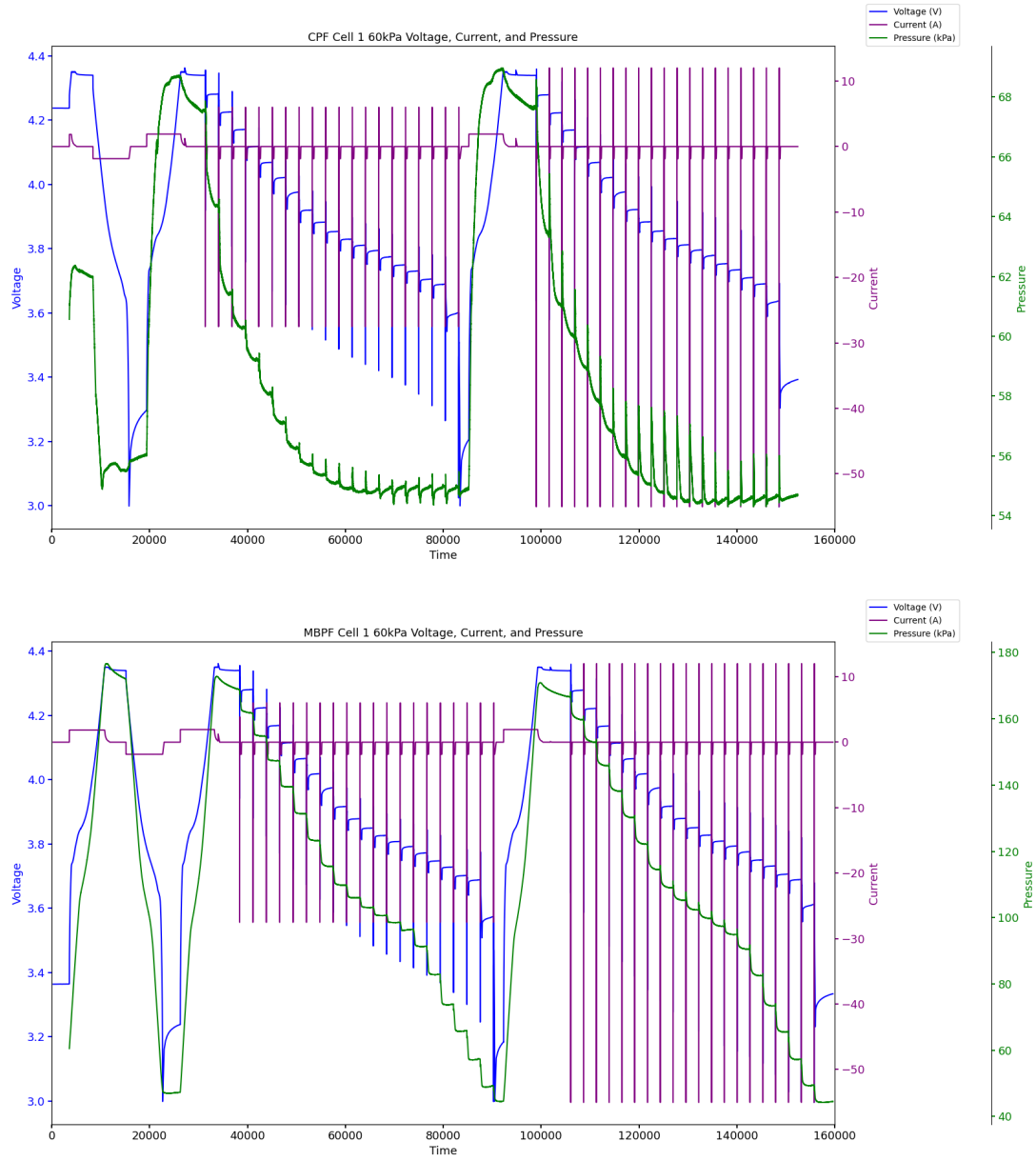


Figure 4: The pressure, voltage, and current throughout the test for CPF (top) and MBPF (bottom) at 60 kPa of stack pressure.

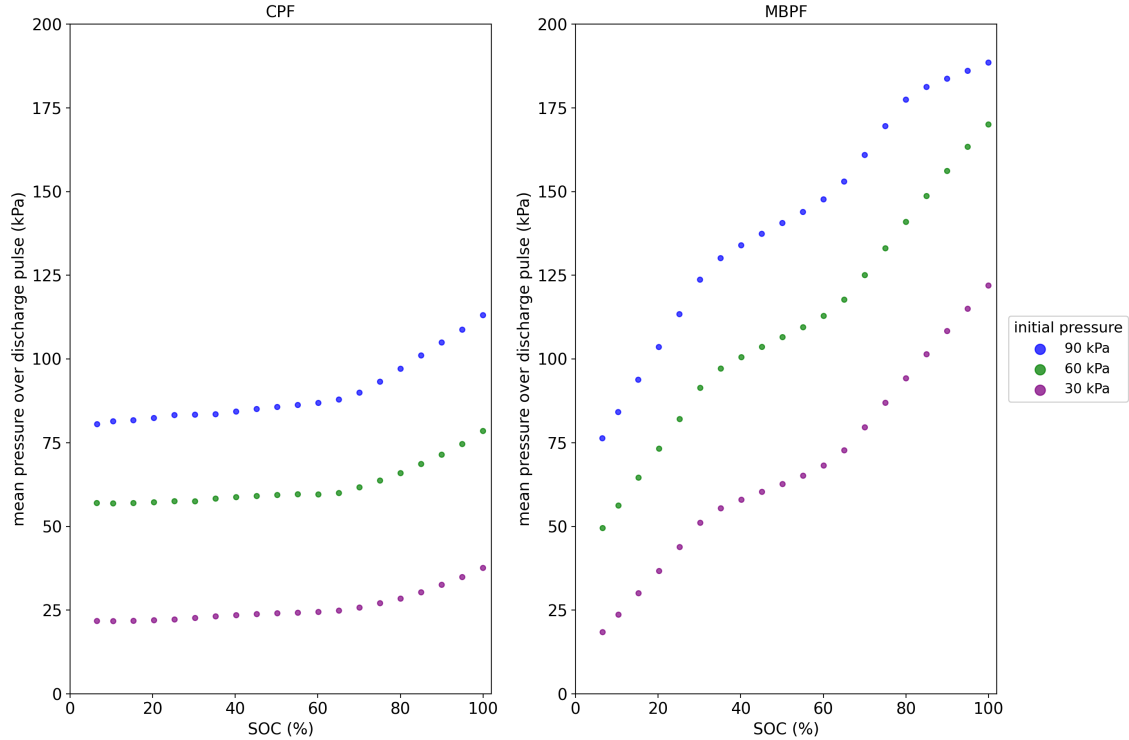


Figure 5: The mean stack pressure for the 10-second discharge pulse for CPF (left) and MBPF (right) for three initial pressures across state-of-charge.

178 The CPF provides a reduction in pressure variance and as such improves future
 179 pouch cell related pressure independence studies. For example, the MBPF stack pressure
 180 increased up to 317% of the initial value for 30 kPa, while the CPF increased by 6%. By
 181 utilising the CPF, variance in pressure has been shown to be within +/- 25%, reducing
 182 pressure variance disruption on results. Since stack pressure has been shown to affect
 183 discharge capacity over cycle life, [3, 5, 12, 17], improved pressure control would enable
 184 pressure invariant isolation of these effects. For example, excessive stack pressures can
 185 lead to crack development in the electrode active material, with the CPF's ability to
 186 adapt to varying thickness this mitigates this mechanism and further provides clarity on
 187 the cell lifetime for a given pressure.

188 Transient pressure variations can occur due to the heat generation occurring inside
 189 the cell. Cells produce heat primarily from joule heating, introduced as,

$$190 \quad Q = I^2 R \quad (1)$$

191 where I is the current through the cell and R is the internal resistance of the cell [33, 34].
 192 As current was applied during the pulses, the cell temperature correspondingly increased.
 193 This results in cell swelling [35, 36] and therefore pressure should the pouch cell have its
 194 displacement constrained. The pressure variance during pulses (Figure 4) was similar
 195 between the MBPF and CPF, although the MBPF did have a higher variance. A reason
 196

197 the CPF may have performed similarly to the MBPF could be its reduced ability to
198 adjust to cell thickness changes in short time frames. Friction between moving and static
199 components may prevent the CPF from adjusting quickly enough to displacement changes
200 to keep stack pressure constant in more transient scenarios. In the case of a battery pack,
201 logging stack pressure to measure transient changes could be useful to gain information
202 on cell energy and heat generation, in addition to temperature management.

203 Additionally, lithium-ion cell thickness growth over time due to SEI layer growth and
204 reduced packing efficiency further emphasises the importance of the CPF for degradation
205 testing. As the cell thickness increases during ageing, a constant displacement constraint
206 would result in rising pressures over time. This could lead to mechanical damage, chem-
207 ical degradation, and premature failure due to excessively increasing stack pressures [7,
208 26]. Using a constant pressure constraint would keep pressures more level even as the cell
209 degrades. This would allow for a more accurate degradation analysis for a given pressure.
210 The CPF could provide the capability of conducting degradation testing at various pres-
211 sures with accurate SOH and failure results. A cycling ageing experiment using the same
212 pressure values and fixtures with a 1C standard charge and discharge could be conducted
213 to compare capacity loss between constant displacement and constant pressure. Fol-
214 lowing the experiment with a postmortem scanning electron microscope, analysis could
215 reveal any physical and chemical degradation effects on cells from the pressure application
216 method.

217 3.2 Cell Performance

218 Throughout this study, DC internal resistance was measured through the HPPC pulse
219 and is defined as,

$$R = \frac{V_f - V_0}{I} \quad (2)$$

221 where V_f is the voltage measured at the end of the 10-second pulse, V_0 is the voltage at
222 the beginning of the pulse and I is the average current applied over the 10-second pulse.
223 A clear difference emerged in both charge and discharge DCIR between the CPF and
224 MBPF while initial pressure varied results for both the CPF and MBPF DCIR. For all
225 initial pressures, the CPF condition generally outperformed the MBPF for both discharge
226 and charge DCIR. Both the CPF and MBPF had the lowest discharge DCIR values at
227 30 and 60 kPa, while the benefits decreased at 90 kPa. The change in DCIR measured
228 by the CPF and MBPF compared to the control condition with 0 kPa of stack pressure
229 can be seen in Figures 6 and 7. The CPF and MBPF results are plotted against each
230 other at each initial pressure for both the D_{\max} cycle and the $D_{\max/2}$ cycle. These plots
231 show the difference in DCIR of the CPF and MBPF compared to the control condition,
232 indicated by the dashed line at $y = 0$.

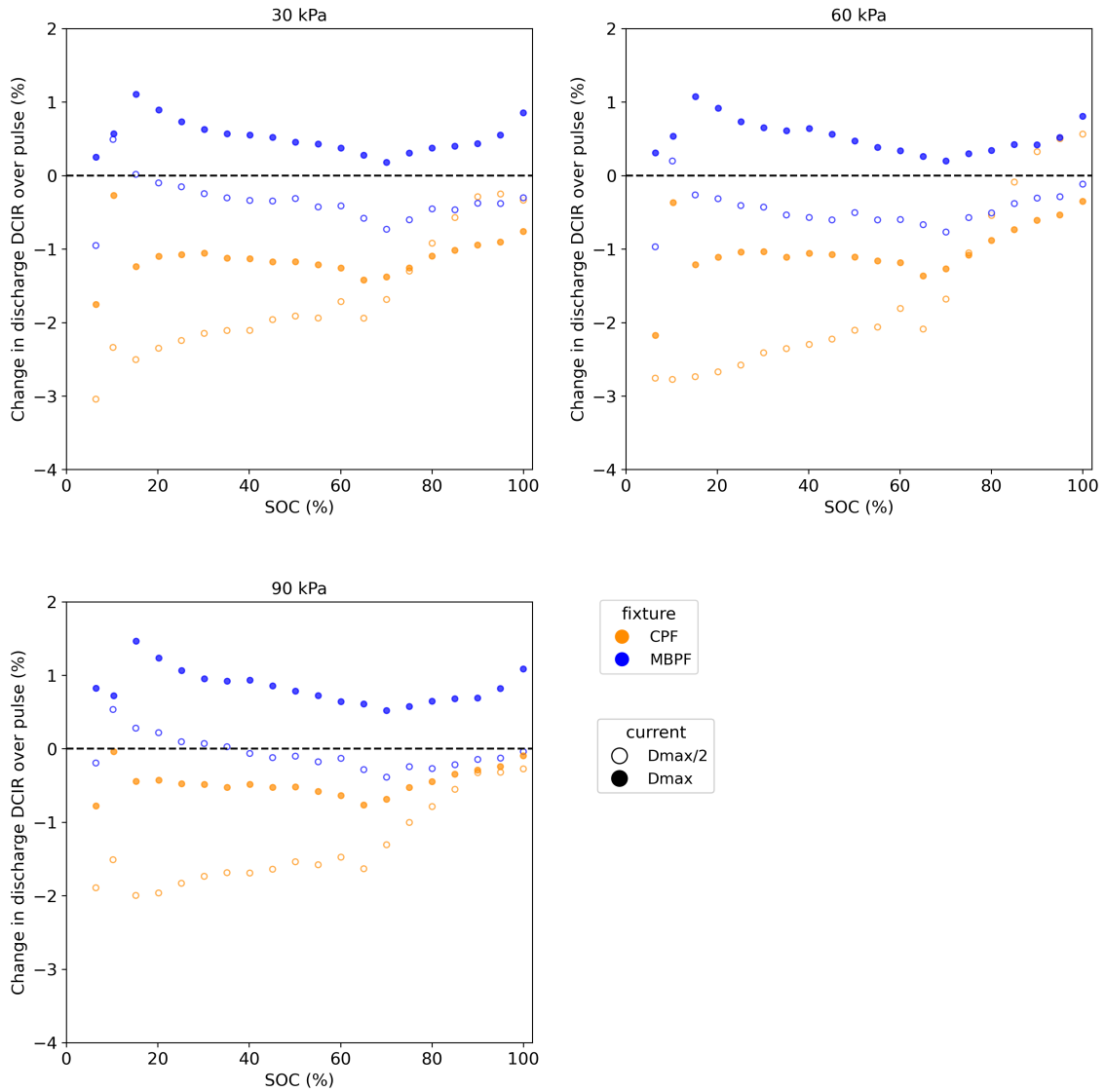


Figure 6: Percent change in discharge DCIR vs SOC for the CPF and MBPF from the control condition at various initial pressures.

Note for Figures 6 and 7: The unconstrained control condition applies 0 kPa of pressure to the cell. The difference in DCIR between each of the two fixtures and the control condition are plotted at each SOC, with the control condition indicated with the dashed line.

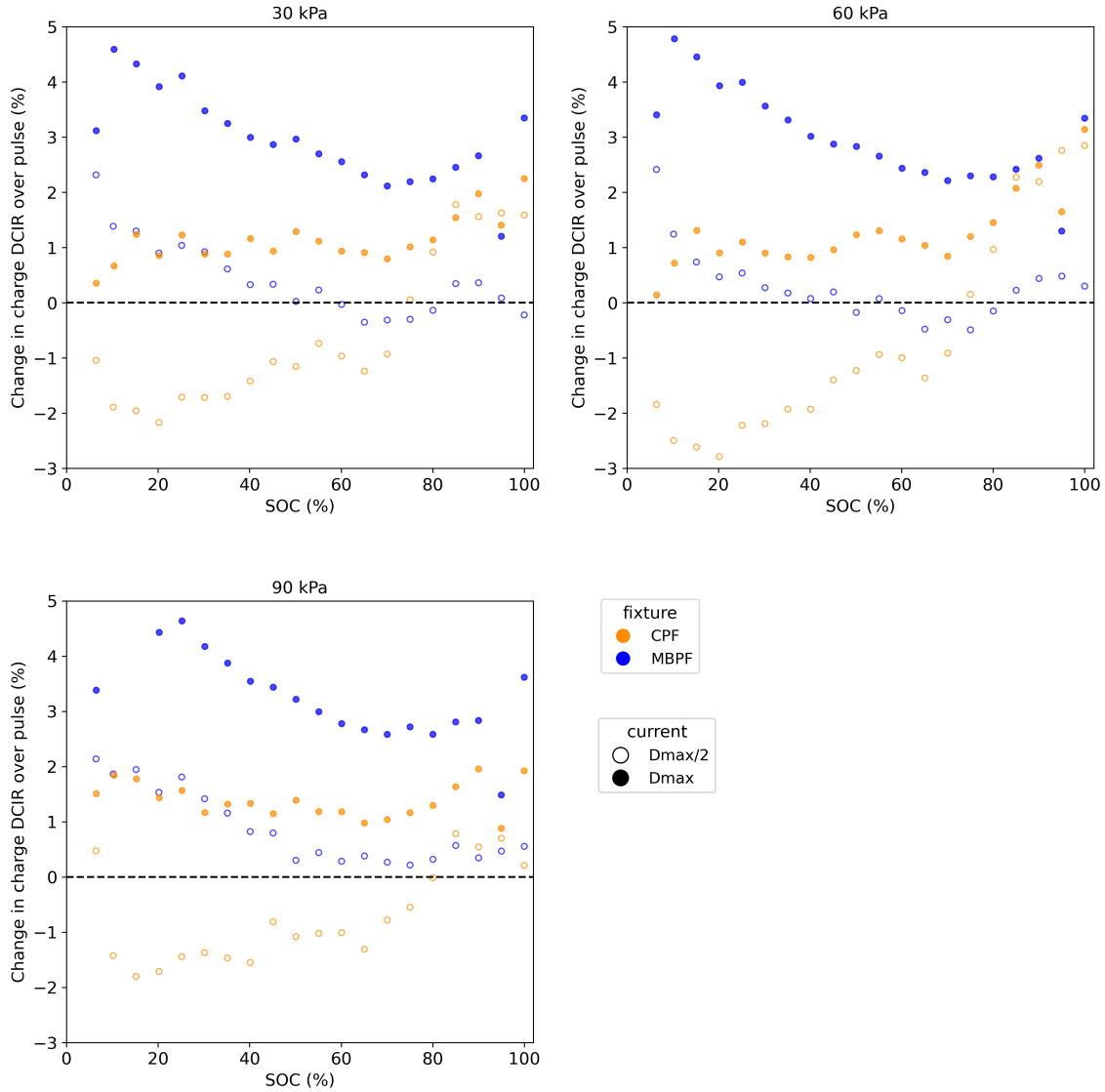


Figure 7: Percent change in charge DCIR vs SOC for the CPF and MBPF from the control condition at various initial pressures.

234 For the discharge pulses (Figure 6), the CPF had lower DCIR than both the MBPF
 235 and control conditions for SOC values below 80%. Above 80% SOC, the CPF only had lower
 236 DCIR at 90 kPa initial pressure. The MBPF generally had lower DCIR than the control
 237 condition in discharge for $D_{\max/2}$, except for 90 kPa. For D_{\max} , the MBPF discharge
 238 DCIR was unanimously higher than the control condition. The CPF stands out as having
 239 lower discharge DCIR than both the MBPF and the 0 kPa condition for all pressures
 240 and both D_{\max} and $D_{\max/2}$. Holding pressure at a level value seemed to reduce discharge
 241 internal resistances, especially at SOC values below 70%. This coincides with the pulse pressure,
 242 as the CPF has a steeper pressure increase at SOC values above 70%. These benefits could come
 243 from effectively increasing surface area through pressure application, without excessively
 244 pressurising the cell. At low SOC values, both the MBPF and CPF had the largest decreases
 245 in internal resistance compared to the 0 kPa test, indicating that applied stack pressure
 246 may have extra benefits at low SOC values. However, low SOC values are the point of the highest

247 DCIR so the normalised difference in DCIR would indicate that the reduction in DCIR
248 is proportional to the nominal value. The lesser difference in discharge DCIR above 70%
249 SOC may be because DCIR is less dependent on pressure at high SOC. Both fixtures
250 had fewer improvements in DCIR from the control condition at D_{\max} . Between 30 and
251 60 kPa seemed optimal for both fixtures in terms of discharge resistance. 90 kPa may
252 be excessively high for the MBPF, as the peak pressure reaching nearly 200 kPa could
253 mitigate the benefits of pressure.

254 For the charge pulses (Figure 7), the CPF generally had lower DCIR than the control
255 condition for $D_{\max/2}$, except for high SOC's where it had higher internal resistances. Both
256 the CPF and MBPF had higher charge DCIR than the control condition for D_{\max} . The
257 MBPF had higher charge internal resistances at lower SOC's than the control condition
258 but had similar charge internal resistances at higher SOC's. The CPF had a lower charge
259 DCIR than the MBPF for nearly all cases, except high SOC's for $D_{\max/2}$. Applied stack
260 pressure could reduce charge performance, which is worse at higher C-rates. Similar
261 to discharge DCIR, the 30 kPa and 60 kPa conditions seem more optimal than 90 kPa
262 stack pressure. Pressure may negatively affect charge resistance due to the decrease in
263 thickness with SOC due to the anode volume change. The applied pressure could be a
264 driving force that biases discharge, as discharging the cell over time decreases thickness.
265 For a 10-second pulse conducted in this study, it is difficult to evaluate if this effect
266 explains the difference in discharge and charge resistance compared to having no stack
267 pressure. The CPF at half the maximum current was the only beneficial condition for
268 charge DCIR. Further investigation into this effect could reveal nuances of the effect of
269 pressure on charge DCIR.

270 The maximum current D_{\max} trial resulted in a lower charge and discharge DCIR for
271 both fixtures and all pressures, including the control. The lower DCIR for the D_{\max} cur-
272 rent cycle could be due to the higher prescribed current changing the plating mechanisms
273 of the electrode [37]. Higher current can accelerate electrochemical processes such as
274 the double layer discharging quicker, reducing the DCIR [38]. This poses an interesting
275 idea that higher current demands could reduce heat generation for pulse conditions in
276 performance settings. This could explain the benefits of pulse charging at certain cur-
277 rents, where resistance is lower than steady charging, improving charging efficiency and
278 fast charging times. The temperature was higher for the D_{\max} condition because higher
279 battery power results in higher heat generation. Since temperature only varied by 1°C,
280 it most likely did not affect the DCIR [37]. Both discharge and charge DCIR had maxi-
281 mum values at the lowest SOC point for all trials. Discharge DCIR values were generally
282 lowest within the 30% to 60% SOC range, while charge DCIR values have a similar dip
283 in the 30% to 60% range, with their lowest value near 100% SOC. DCIR increased at
284 low SOC due to the reduction in available intercalation space in the cathode. Diffusion
285 becomes more difficult as more lithium ions occupy available space in the cathode ma-
286 terial, increasing resistance. Inversely, the charge DCIR increased at high SOC, due to
287 the increased difficulty of intercalating lithium into the negative electrode. The charge
288 DCIR had less of a resistance increase, which aligns with previous studies [39–41].

289 Power differences were also measured between the fixtures. Figures 8 and 9 show the
290 power plotted as a difference in discharge and charge power at various pressures compared
291 to the control baseline, shown by the dashed line at $y = 0$. Generally, both the discharge
292 and charge power increased with SOC, but the charge power was lowest at 95% SOC.
293 Power increased with SOC due to the cell voltage vs SOC. Discharge power at low SOC
294 and charge power at high SOC were both important metrics because minimum voltage
295 and maximum voltage limit the power, respectively. At high SOCs, being able to keep cell
296 voltage below the maximum cutoff voltage enables faster charging, while at low SOCs,
297 maintaining a voltage above the minimum cut-off voltage enables higher discharge power.
298 The CPF had higher discharge power than both the MBPF and control case for nearly
299 all pressures and SOCs, except for 60 kPa of stack pressure. Increasing discharge current
300 increased the difference in discharge power between the CPF and MBPF to the control
301 condition. The CPF had greater power benefits at the higher current, while the MBPF
302 had greater power detriments. The greater difference between the CPF and MBPF
303 at D_{\max} reveals that constant pressure could be more beneficial in terms of discharge
304 power at high C-rates. The MBPF performed worse at higher C-rates, indicating that
305 constraining displacement can be detrimental to cell performance in this scenario. The
306 CPF had the largest increase of power at low SOCs, except for the 90 kPa condition. The
307 CPF achieved a power difference on the last discharge pulse of over 3 W compared to 0
308 kPa and 5 W compared to the MBPF when both fixtures were tested at 60 kPa. The
309 CPF saw this smallest increase of power at 90 kPa, possibly due to pressure exceeding
310 the limit of benefit for the cell. Similarly to DCIR, differences in charge power were less
311 significant between the fixtures than discharge power. Both the CPF and MBPF had less
312 charge power at high SOCs than the control condition, and slightly more charge power
313 at low SOC. The loss of charge power at high SOC could be because of the previously
314 mentioned idea that pressure can be adverse for charging in some cases. The MBPF had
315 an edge over the CPF for charge power, especially at low SOCs for D_{\max} . The CPF had
316 less charge power than the control case for low SOCs at D_{\max} , performing worst at 90
317 kPa.

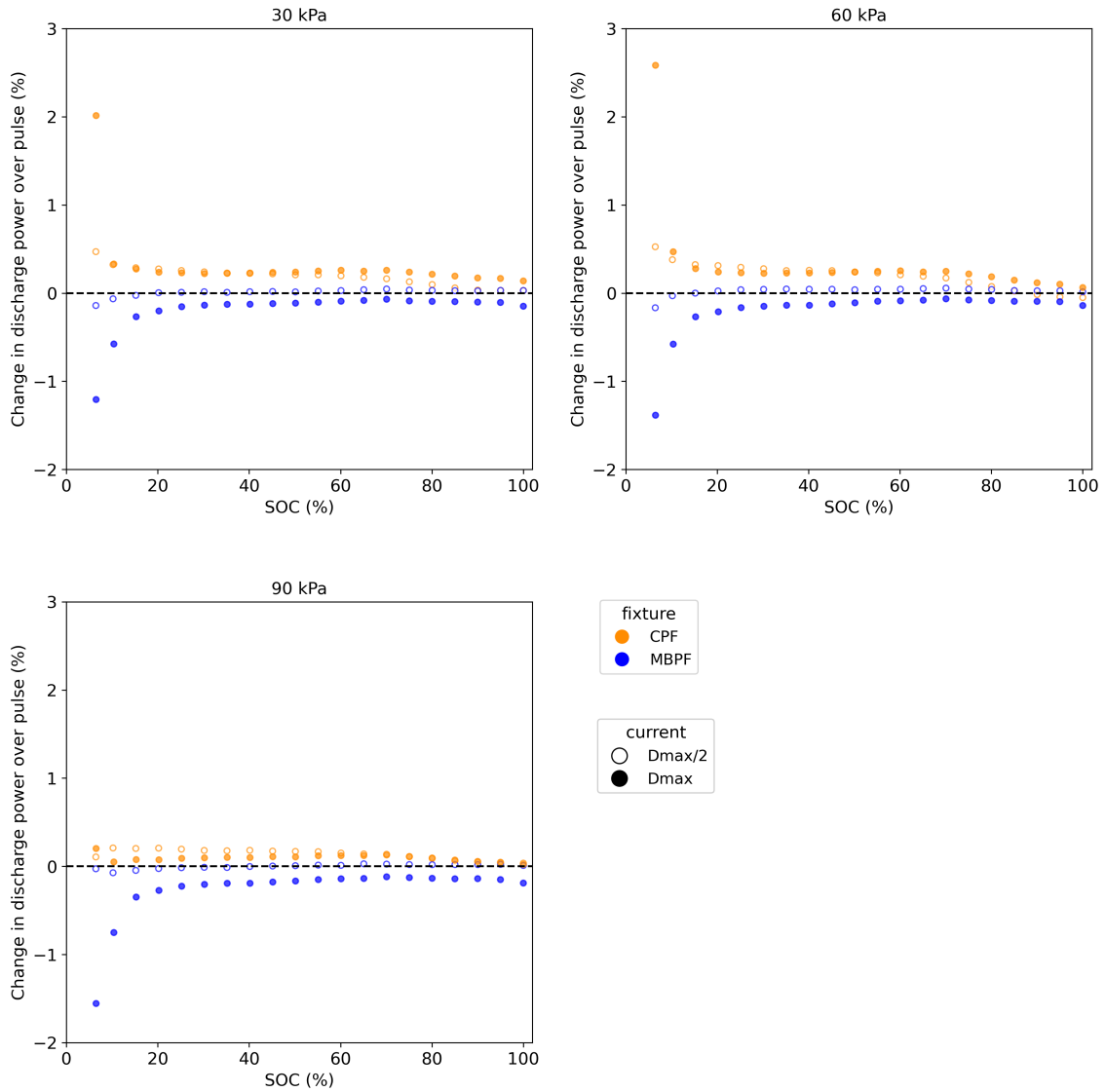


Figure 8: Percent change in discharge power vs SOC for the CPF and MBPF from the control condition at various initial pressures.

Note for Figures 8 and 9: The unconstrained control condition applies 0 kPa of pressure to the cell. The difference in power between each of the two fixtures and the control condition are plotted at each SOC, with the control condition indicated with the dashed line.

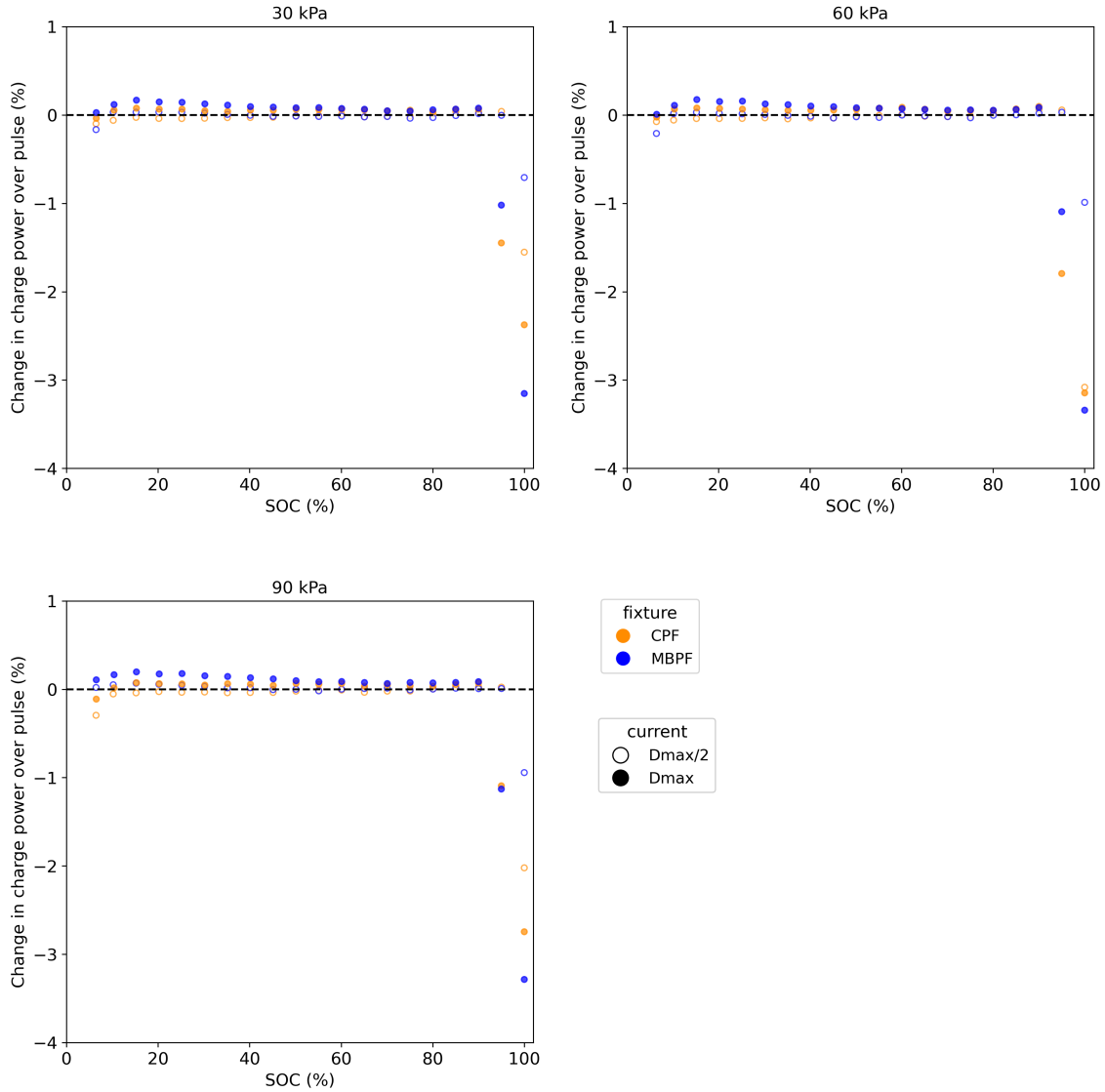


Figure 9: Percent change in charge power vs SOC for the CPF and MBPF from the control condition at various initial pressures.

318 Discharge capacity ranged from 3.84–3.86 Ah, for all fixtures constraints and for the
 319 control. Given that the differences in discharge capacity were less than 1%, there is
 320 not enough evidence to show that stack pressure affected discharge capacity in the short
 321 term. Lithium-ion pouch cells may not benefit from the capacity increase from stack
 322 pressure as with lithium-metal anode and silicon-blend anode cells, where much higher
 323 stack pressures showed improvements in capacity [19, 26]. Hahn et al. [1] found that
 324 stack pressure decreased lithium-ion cell capacity initially, then provided better capacity
 325 retention during calendar ageing. The possible benefits of dendrite growth suppression,
 326 gas suppression, and SEI layer growth suppression would only emerge with degradation
 327 testing and/or calendar ageing.

328 4 Conclusion

329 A fixture was developed to evaluate the effects of constant pressure and constant displace-
330 ment constraints on cell performance. The designed fixture performed as expected with
331 pressure variations of below 25% when compared to a conventional fixed-displacement
332 system with a pressure variation of over 300%. Improvements in discharge resistance
333 and power were observed by applying constant pressure with no significant capacity or
334 Coulombic efficiency differences were measured. Incorporating more uniform pressure on
335 pouch cells independent of cell swelling could improve discharge capabilities for perfor-
336 mance scenarios. Designing battery packs that pressurize pouch cells while allowing them
337 to expand and contract could improve the discharge power of packs, an important metric
338 for performance scenarios. Additionally, lower discharge internal resistance would reduce
339 power loss during discharge, improving vehicle performance.

340 Further work could reduce errors from sensors and mechanical flex to obtain higher
341 fidelity data. The load cells measuring the pressure did have signal noise, although
342 this was seen to be less than the change in pressures during the discharge and charge
343 pulses. Nevertheless, hysteresis error and random error could have affected the pressure
344 results. Incorporating a singular, more accurate load cell could improve the resolution
345 and accuracy of the pressure data. Flexing in the pressure plates was seen during testing
346 for both the CPF and MBPF, and was more noticeable at 90 kPa. This deformation
347 could have negatively impacted pressure distribution, reducing the possible benefits of
348 stack pressure. Selecting a different design for the plates in terms of materials or geometry
349 could mitigate this possible source of error. Testing cell degradation with both fixtures
350 could reveal possible long-term capacity benefits from applying constant stack pressure.

References

- [1] Severin Hahn et al. “Pressure Prediction Modeling and Validation for Lithium-Ion Pouch Cells in Buffered Module Assemblies”. In: *Journal of Energy Storage* 40 (2021), p. 102517. ISSN: 2352-152X. DOI: <https://doi.org/10.1016/j.est.2021.102517>. URL: <https://www.sciencedirect.com/science/article/pii/S2352152X21002656>.
- [2] Yihui Jiang et al. “A stack pressure based equivalent mechanical model of lithium-ion pouch batteries”. In: *Energy* 221 (2021), p. 119804. ISSN: 0360-5442. DOI: <https://doi.org/10.1016/j.energy.2021.119804>. URL: <https://www.sciencedirect.com/science/article/pii/S0360544221000530>.
- [3] Abdilbari Shifa Mussa et al. “Effects of external pressure on the performance and ageing of single-layer lithium-ion pouch cells”. en. In: *Journal of Power Sources* 385 (May 2018), pp. 18–26. ISSN: 03787753. DOI: [10.1016/j.jpowsour.2018.03.020](https://doi.org/10.1016/j.jpowsour.2018.03.020). URL: <https://linkinghub.elsevier.com/retrieve/pii/S0378775318302441> (visited on 07/18/2021).
- [4] Long Zhou et al. “A study of external surface pressure effects on the properties for lithium-ion pouch cells”. In: *International Journal of Energy Research* 44.8 (2020), pp. 6778–6791.
- [5] Verena Müller et al. “Study of the influence of mechanical pressure on the performance and aging of Lithium-ion battery cells”. In: *Journal of Power Sources* 440 (2019), p. 227148. DOI: <https://doi.org/10.1016/j.jpowsour.2019.227148>.
- [6] Ruihe Li et al. “Effect of external pressure and internal stress on battery performance and lifespan”. In: *Energy Storage Materials* 52 (2022), pp. 395–429. ISSN: 2405-8297. DOI: <https://doi.org/10.1016/j.ensm.2022.07.034>. URL: <https://www.sciencedirect.com/science/article/pii/S2405829722004044>.
- [7] John Cannarella and Craig B. Arnold. “Stress evolution and capacity fade in constrained lithium-ion pouch cells”. In: *Journal of Power Sources* 245 (2014), pp. 745–751. ISSN: 0378-7753. DOI: <https://doi.org/10.1016/j.jpowsour.2013.06.165>. URL: <https://www.sciencedirect.com/science/article/pii/S037877531301197X>.
- [8] Christina Peabody and Craig B. Arnold. “The role of mechanically induced separator creep in lithium-ion battery capacity fade”. In: *Journal of Power Sources* 196.19 (2011), pp. 8147–8153. ISSN: 0378-7753. DOI: <https://doi.org/10.1016/j.jpowsour.2011.05.023>. URL: <https://www.sciencedirect.com/science/article/pii/S037877531100989X>.

- 386 [9] Shaojun Niu et al. “Analysis on the effect of external press force on the performance
387 of LiNi_{0.8}Co_{0.1}Mn_{0.1}O₂/Graphite large pouch cells”. In: *Journal of Energy Storage*
388 44 (2021), p. 103425. ISSN: 2352-152X. DOI: [https://doi.org/10.1016/j.est.
389 2021.103425](https://doi.org/10.1016/j.est.2021.103425). URL: [https://www.sciencedirect.com/science/article/pii/
390 S2352152X21011117](https://www.sciencedirect.com/science/article/pii/S2352152X21011117).
- 391 [10] John Cannarella and Craig B. Arnold. “State of health and charge measurements
392 in lithium-ion batteries using mechanical stress”. In: *Journal of Power Sources* 269
393 (2014), pp. 7–14. ISSN: 0378-7753. DOI: [https://doi.org/10.1016/j.jpowsour.
394 2014.07.003](https://doi.org/10.1016/j.jpowsour.2014.07.003). URL: [https://www.sciencedirect.com/science/article/pii/
395 S0378775314010453](https://www.sciencedirect.com/science/article/pii/S0378775314010453).
- 396 [11] AJ Louli, LD Ellis, and JR Dahn. “Operando pressure measurements reveal solid
397 electrolyte interphase growth to rank Li-ion cell performance”. In: *Joule* 3.3 (2019),
398 pp. 745–761.
- 399 [12] Emanuele Micheli et al. “Experimental Investigation on Reversible Swelling Mech-
400 anisms of Lithium-Ion Batteries under a Varying Preload Force”. In: *Batteries* 9.4
401 (2023). ISSN: 2313-0105. DOI: [10.3390/batteries9040218](https://doi.org/10.3390/batteries9040218). URL: [https://www.
402 mdpi.com/2313-0105/9/4/218](https://www.mdpi.com/2313-0105/9/4/218).
- 403 [13] Jean-Marie Doux et al. “Pressure effects on sulfide electrolytes for all solid-state
404 batteries”. In: *J. Mater. Chem. A* 8 (10 2020), pp. 5049–5055. DOI: [10.1039/
405 C9TA12889A](https://doi.org/10.1039/C9TA12889A).
- 406 [14] Wesley Chang et al. “Evolving contact mechanics and microstructure formation dy-
407 namics of the lithium metal-Li₇La₃Zr₂O₁₂ interface”. In: *Nature Communications*
408 12 (Nov. 2021), p. 6369. DOI: [10.1038/s41467-021-26632-x](https://doi.org/10.1038/s41467-021-26632-x).
- 409 [15] Xin Zhang et al. “Pressure-Driven Interface Evolution in Solid-State Lithium Metal
410 Batteries”. In: *Cell Reports Physical Science* 1.2 (2020), p. 100012. ISSN: 2666-
411 3864. DOI: <https://doi.org/10.1016/j.xcrp.2019.100012>. URL: [https :
412 //www.sciencedirect.com/science/article/pii/S266638641930013X](https://www.sciencedirect.com/science/article/pii/S266638641930013X).
- 413 [16] Alexander J Louli et al. “Exploring the impact of mechanical pressure on the per-
414 formance of anode-free lithium metal cells”. In: *Journal of The Electrochemical*
415 *Society* 166.8 (2019), A1291–A1299.
- 416 [17] Cameron Martin et al. “Cycling Lithium Metal on Graphite to Form Hybrid Lithium-
417 Ion/Lithium Metal Cells”. In: *Joule* 4 (2020), pp. 1296–1310. DOI: [https://doi .
418 org/10.1016/j.joule.2020.04.003](https://doi.org/10.1016/j.joule.2020.04.003).
- 419 [18] Gregory L Plett. *Battery management systems. Volume I, Battery modeling*. Tech-
420 nology & Engineering, 2015.
- 421 [19] Gert Berkmans et al. “Electrical Characterization and Micro X-ray Computed To-
422 mography Analysis of Next-Generation Silicon Alloy Lithium-Ion Cells”. In: *World*
423 *Electric Vehicle Journal* 9.3 (2018). ISSN: 2032-6653. DOI: [10.3390/wevj9030043](https://doi.org/10.3390/wevj9030043).
424 URL: <https://www.mdpi.com/2032-6653/9/3/43>.

- 425 [20] Charles Monroe and John Newman. “The Effect of Interfacial Deformation on Elec-
426 trodeposition Kinetics”. In: *Journal of The Electrochemical Society* 151 (June 2004),
427 A880–A886. DOI: [10.1149/1.1710893](https://doi.org/10.1149/1.1710893).
- 428 [21] Sangil Hyun and Mark O. Robbins. “Elastic contact between rough surfaces: Effect
429 of roughness at large and small wavelengths”. In: *Tribology International* 40.10
430 (2007). Tribology at the Interface: Proceedings of the 33rd Leeds-Lyon Symposium
431 on Tribology (Leeds, 2006), pp. 1413–1422. ISSN: 0301-679X. DOI: <https://doi.org/10.1016/j.triboint.2007.02.003>. URL: <https://www.sciencedirect.com/science/article/pii/S0301679X07000369>.
- 434 [22] Joachim Larsson, Shiro Biwa, and Bertil Storåkers. “Inelastic flattening of rough
435 surfaces”. In: *Mechanics of Materials* 31.1 (1999), pp. 29–41. ISSN: 0167-6636. DOI:
436 [https://doi.org/10.1016/S0167-6636\(98\)00046-5](https://doi.org/10.1016/S0167-6636(98)00046-5). URL: <https://www.sciencedirect.com/science/article/pii/S0167663698000465>.
- 438 [23] H. M. Stanley and T. Kato. “An FFT-Based Method for Rough Surface Con-
439 tact”. In: *Journal of Tribology* 119.3 (July 1997), pp. 481–485. ISSN: 0742-4787.
440 DOI: [10.1115/1.2833523](https://doi.org/10.1115/1.2833523). eprint: https://asmedigitalcollection.asme.org/tribology/article-pdf/119/3/481/5602831/481_1.pdf. URL: <https://doi.org/10.1115/1.2833523>.
- 443 [24] Shashank Arora, Weixiang Shen, and Ajay Kapoor. “Review of mechanical design
444 and strategic placement technique of a robust battery pack for electric vehicles”. In:
445 *Renewable and Sustainable Energy Reviews* 60 (2016), pp. 1319–1331. ISSN: 1364-
446 0321. DOI: <https://doi.org/10.1016/j.rser.2016.03.013>. URL: <https://www.sciencedirect.com/science/article/pii/S1364032116002483>.
- 448 [25] Lip Huat Saw, Yonghuang Ye, and Andrew A.O. Tay. “Integration issues of lithium-
449 ion battery into electric vehicles battery pack”. In: *Journal of Cleaner Production*
450 113 (2016), pp. 1032–1045. ISSN: 0959-6526. DOI: <https://doi.org/10.1016/j.jclepro.2015.11.011>. URL: <https://www.sciencedirect.com/science/article/pii/S0959652615016406>.
- 453 [26] Gert Berckmans et al. “Analysis of the effect of applying external mechanical pres-
454 sure on next generation silicon alloy lithium-ion cells”. In: *Electrochimica Acta*
455 306 (2019), pp. 387–395. ISSN: 0013-4686. DOI: <https://doi.org/10.1016/j.electacta.2019.03.138>. URL: <https://www.sciencedirect.com/science/article/pii/S0013468619305614>.
- 458 [27] Lysander De Sutter et al. “Mechanical behavior of Silicon-Graphite pouch cells
459 under external compressive load: Implications and opportunities for battery pack
460 design”. In: *Journal of Power Sources* 451 (2020), p. 227774. ISSN: 0378-7753. DOI:
461 <https://doi.org/10.1016/j.jpowsour.2020.227774>. URL: <https://www.sciencedirect.com/science/article/pii/S037877532030077X>.

- 463 [28] Bernhard Bitzer and Andreas Gruhle. “A new method for detecting lithium plat-
464 ing by measuring the cell thickness”. In: *Journal of Power Sources* 262 (2014),
465 pp. 297–302. ISSN: 0378-7753. DOI: [https://doi.org/10.1016/j.jpowsour.](https://doi.org/10.1016/j.jpowsour.2014.03.142)
466 [2014.03.142](https://doi.org/10.1016/j.jpowsour.2014.03.142). URL: [https://www.sciencedirect.com/science/article/pii/](https://www.sciencedirect.com/science/article/pii/S0378775314004753)
467 [S0378775314004753](https://www.sciencedirect.com/science/article/pii/S0378775314004753).
- 468 [29] Davide Clerici, Francesco Mocera, and Aurelio Somà. “Electrochemical–mechanical
469 multi-scale model and validation with thickness change measurements in prismatic
470 lithium-ion batteries”. In: *Journal of Power Sources* 542 (2022), p. 231735. ISSN:
471 0378-7753. DOI: <https://doi.org/10.1016/j.jpowsour.2022.231735>. URL:
472 <https://www.sciencedirect.com/science/article/pii/S0378775322007297>.
- 473 [30] B. Rieger et al. “Multi-scale investigation of thickness changes in a commercial
474 pouch type lithium-ion battery”. In: *Journal of Energy Storage* 6 (2016), pp. 213–
475 221. ISSN: 2352-152X. DOI: <https://doi.org/10.1016/j.est.2016.01.006>. URL:
476 <https://www.sciencedirect.com/science/article/pii/S2352152X16300068>.
- 477 [31] Katie Lukow. *MBPF*. 2022. DOI: <https://doi.org/10.5281/zenodo.7509368>.
478 URL: <https://github.com/katielukow/MBPF>.
- 479 [32] High Voltage Energy Storage Group. *Battery Testing Consortium Protocol*. 2022.
480 URL: <https://github.com/HVES-Battery-Testing-Consortium/LG-HG2>.
- 481 [33] V.G. Choudhari, Dr A.S. Dhoble, and T.M. Sathe. “A review on effect of heat
482 generation and various thermal management systems for lithium ion battery used
483 for electric vehicle”. In: *Journal of Energy Storage* 32 (2020), p. 101729. ISSN:
484 2352-152X. DOI: <https://doi.org/10.1016/j.est.2020.101729>. URL: [https://](https://www.sciencedirect.com/science/article/pii/S2352152X20315668)
485 www.sciencedirect.com/science/article/pii/S2352152X20315668.
- 486 [34] Yongqi Xie et al. “Experimental and analytical study on heat generation character-
487 istics of a lithium-ion power battery”. In: *International Journal of Heat and Mass*
488 *Transfer* 122 (2018), pp. 884–894. ISSN: 0017-9310. DOI: [https://doi.org/10.](https://doi.org/10.1016/j.ijheatmasstransfer.2018.02.038)
489 [1016/j.ijheatmasstransfer.2018.02.038](https://doi.org/10.1016/j.ijheatmasstransfer.2018.02.038). URL: [https://www.sciencedirect.](https://www.sciencedirect.com/science/article/pii/S001793101733421X)
490 [com/science/article/pii/S001793101733421X](https://www.sciencedirect.com/science/article/pii/S001793101733421X).
- 491 [35] Ki-Yong Oh and Bogdan I. Epureanu. “A novel thermal swelling model for a
492 rechargeable lithium-ion battery cell”. In: *Journal of Power Sources* 303 (2016),
493 pp. 86–96. ISSN: 0378-7753. DOI: [https://doi.org/10.1016/j.jpowsour.](https://doi.org/10.1016/j.jpowsour.2015.10.085)
494 [2015.10.085](https://doi.org/10.1016/j.jpowsour.2015.10.085). URL: [https://www.sciencedirect.com/science/article/pii/](https://www.sciencedirect.com/science/article/pii/S0378775315304730)
495 [S0378775315304730](https://www.sciencedirect.com/science/article/pii/S0378775315304730).
- 496 [36] Yan Zhao et al. “Localized swelling inhomogeneity detection in lithium ion cells
497 using multi-dimensional laser scanning”. In: *Journal of The Electrochemical Society*
498 166.2 (2019), A27.
- 499 [37] Anup Barai et al. “A study of the influence of measurement timescale on internal
500 resistance characterisation methodologies for lithium-ion cells”. In: *Scientific reports*
501 8.1 (2018), pp. 1–13.

- 502 [38] Wladislaw Waag, Stefan Käbitz, and Dirk Uwe Sauer. “Experimental investiga-
503 tion of the lithium-ion battery impedance characteristic at various conditions and
504 aging states and its influence on the application”. In: *Applied Energy* 102 (2013).
505 Special Issue on Advances in sustainable biofuel production and use - XIX In-
506 ternational Symposium on Alcohol Fuels - ISAF, pp. 885–897. ISSN: 0306-2619.
507 DOI: <https://doi.org/10.1016/j.apenergy.2012.09.030>. URL: <https://www.sciencedirect.com/science/article/pii/S030626191200671X>.
508
- 509 [39] Tobias Teuffl et al. “State of charge dependent resistance build-up in Li-and Mn-
510 rich layered oxides during lithium extraction and insertion”. In: *Journal of The*
511 *Electrochemical Society* 166.6 (2019), A1275.
- 512 [40] Jianming Zheng et al. “Electrochemical kinetics and performance of layered compos-
513 ite cathode material Li [Li_{0.2}Ni_{0.2}Mn_{0.6}]O₂”. In: *Journal of The Electrochemical*
514 *Society* 160.11 (2013), A2212.
- 515 [41] Sanketh R Gowda et al. “Examining the electrochemical impedance at low states
516 of charge in lithium-and manganese-rich layered transition-metal oxide electrodes”.
517 In: *Journal of The Electrochemical Society* 162.7 (2015), A1374.

518 Data Availability

519 For questions in regard to obtaining test data, please contact the High Voltage Energy
520 Storage group at Oxford Brookes University: <https://hves.brookes.ac.uk>.